Wang, Winslow, et al. Published in Journal of Power Sources, 268, 246-254. June 13, 2014.

Development of MnO_2 cathode inks for flexographically printed rechargeable zinc-based battery

Zuoqian Wang [a, *], Rich Winslow [b], Deepa Madan [b], Paul K. Wright [b], James W. Evans [c], Malcolm Keif [d], Xiaoying Rong [d]

[a] *Applied Materials, Inc., Santa Clara, CA, USA*
[b] *Department of Mechanical Engineering, University of California, Berkeley, CA, USA*
[c] *Department of Materials Science and Engineering, University of California, Berkeley, CA, USA*
[d] *Graphic Communication Department, Cal Poly State University, San Luis Obispo, CA, USA*

HIGHLIGHTS

- A flexographic printing method for battery fabrication was presented.
- Key criteria for developing functional flexographic inks were established.
- A variety of MnO_2 composite cathode inks were developed and analyzed.
- A PSBR based ink showed excellent printability and electrochemical performance.

ABSTRACT

A novel roll-to-roll flexographic printing process for rechargeable zinc-based battery manufacturing was presented in this paper. Based on the fundamental operating mechanism of flexography, key criteria for developing functional flexographic printing inks were established, including composite ink rheology (steady-state viscosity and yield stress), ink wettability as well as ink dispersing qualities. A variety of MnO_2 cathode inks were developed and analyzed comprehensively based on these criteria. A novel type of aqueous cathode ink based on PSBR polymeric binder showed excellent flexographic printability as well as promising electrochemical performance.

1. Introduction

Long-life, energy dense, low-cost, flexible electrochemical energy storage systems have become a fast-emerging industry in recent decades, with potential applications from wireless sensor networks, [1–8] portable electronics, [9,10] electric vehicles [11–13] to grid energy storage [14–17], ranging from mW to MW scales. Both a fundamental breakthrough in battery chemistry and major innovations in fabrication methods are needed to significantly reduce battery cost, and to allow for easier integration with such a wide variety of applications.

Significant research efforts in the battery field have recently been made towards development of rechargeable zinc battery chemistries, motivated primarily by their high energy and power densities, inherent safety, low toxicity, relative ease in handling, and low cost. [18–21] Specifically, rechargeable nickel–zinc, [22,23] silver–zinc, [24] alkaline manganese dioxide (MnO_2)-zinc [25] and zinc-air [26,27] batteries have been studied. A printable zinc–manganese dioxide(MnO_2) microbattery was developed in previous research [21,28] for wireless sensor network applications, based on a novel ionic liquid 1-butyl-3-methylimidazolium trifluoromethanesulfonate (BMIM + Tf-) gel electrolyte. It has been shown by Ho [21] that MnO_2 appeared to be an reversible intercalation host for zinc ions, and served as a good cathode material in a zinc-metal oxide battery. The first microbattery prototype shows promising properties, with the cell exhibiting storage capacities of

* Corresponding author.
E-mail address: wangjoaking@gmail.com (Z. Wang).

about 1 mAh cm^{-2} over more than 70 cycles. [21] A novel dispenser printing method was developed and utilized for additive manufacturing of the sandwich structured battery. The custom-built dispenser printer demonstrated great flexibility and precision in energy harvesting and energy storage device fabrication for prototyping. Research on electrochemical capacitors, [29,30] thermoelectric generators [6,31–38] as well as MEMS current sensors [39] have been also conducted using this versatile prototype dispenser printer. However, due to the limitations of this printer, only mm to cm scale batteries can be printed, even then at relatively low throughput rates, which is good for device prototyping but not for large-scale manufacturing.

A roll-to-roll printing process has therefore been proposed for the developed battery technology using commercially available flexographic printing presses, as shown in Fig. 1. Flexography is traditionally used for printing packages, newspapers and magazines. It was selected for scalable battery manufacturing because of its great advantages: it is a fully automatic process with high throughput rate; it is a mature wide web process – thus good for large-format device printing; it has flexible, soft plates thus it has great flexibility with the printing substrates including metal foils; it can print at resolution as low as 20 μm–30 μm, which is good enough for battery applications. Each of the four stations is designed to print or deposit the developed functional inks for the cathode, electrolyte, anode and current collector in series, respectively. Printing plates are designed to print the various components of custom-sized batteries in custom patterns, eventually forming a sandwich-structured battery. This roll-to-roll manufacturing technology is capable of fabricating batteries with capacities ranging from mA-hrs (microbatteries) to A-hrs (grid-scale batteries).

There are previous studies, including multiple patents from Bjorksten [40], Story [41] and Bergum [42], on printable batteries as well as electrode ink formulations. However, as far as the authors know, there are no fundamental and systematic studies on the composite electrode ink development, especially for flexographic printing method. Different flexographic manufacturing process parameters, such as alignment, printing speed, drying techniques, intensity and time should be strictly designed at each printing station depending on the formulations of the functional ink to provide optimized printing quality and battery performance. What turns out to be most critical is to develop functional inks with suitable fluidic properties for this unique high-speed ink transfer process in order to achieve excellent printing quality. Large volumes of inks (in liters) are typically needed to fill the ink reservoir for a cost effective process, so the inks need to maintain high dispersing qualities and have minimal aging effect. Because the inks need to be transferred effectively at high speed from the ink reservoir to the substrate through multiple rollers and media, including rubber fountain rollers, ceramic anilox rollers as well as photopolymer plates, the viscosity and wetting properties must be well adjusted so that a high ink transfer rate and accuracy are achieved. Once the inks are transferred to a variety of substrates, both a compressive force from the impression cylinder as well as a shear force due to the relative motion of the substrates and plates are applied to the inks, so the inks need also to have proper structural properties to form desired pattern with high accuracy.

Because flexographic printing presses are designed for large volume manufacturing, aqueous-based inks are highly desired due to environmental, safety and cost concerns, compared to traditional organic solvent based formulations for battery chemistry and have therefore been the main subject of this investigation. In the previous work, a cathode slurry was developed based on traditional Poly(vinylidene fluoride-co-hexafluoropropene) (PVDF-HFP) binding material, which requires volatile n-methyl-2-pyrrolidone (NMP) as the solvent. [43] Water-soluble binder systems such as sodium salt of carboxymethyl cellulose (CMC) and styrene-butadiene rubber (SBR) have been recently introduced in the manufacturing of lithium ion battery electrodes. [44–47] This work explores the application of various water-based CMC/SBR binder formulations as well as water-based single modified SBR (PSBR) binding solution, in the zinc-based battery chemistry and electrode fabrication using flexographic printing technology.

Inks developed previously for the custom dispenser printer show various poor printing qualities on flexographic printing press. Among them, poor wetting shown in Fig. 2(b) was typically due to the high surface tension of the inks relative to the low surface energy of the foil substrate, especially for some aqueous-based composite inks; Non-uniformity as shown in Fig. 2(c) happened frequently with low viscosity NMP-based inks with poor structural properties. Active particles in the cathode slurry were easily squeezed to the edge of the square on the stainless steel substrate instead of spreading uniformly. Comparing to what we obtained from using commercial graphic black inks (inks used for printing newspapers etc) in Fig. 2(a), it was concluded that substantial ink fluidic property analysis and improvements, beyond inks developed for dispenser printing, are necessary to achieve high quality functional thick films from flexographic printing. In the following sections, the rheology and wettability as well as dispersion analysis focused on a variety of synthesized cathode inks will be discussed. Physical characterizations of the dried cathode films were performed and correlated to the ink formulations and properties. With good battery cathode films flexographically printed, electrochemical characterizations were then conducted for further optimization of the battery chemistry.

2. Experimental

2.1. Composite ink development and preparations

2.1.1. Commercial flexographic graphic inks (Performa Ink System) were directly ordered from Actega WIT, Inc. The specific graphic ink used for this work is water-based black ink.

2.1.2. A type of composite ink based on commercial extender solution was developed with active cathode powders. The formulation includes 90 wt% activated MnO_2 powder with particle sizes <5 μm (Sigma–Aldrich), 6 wt% acetylene black (AB) conductive

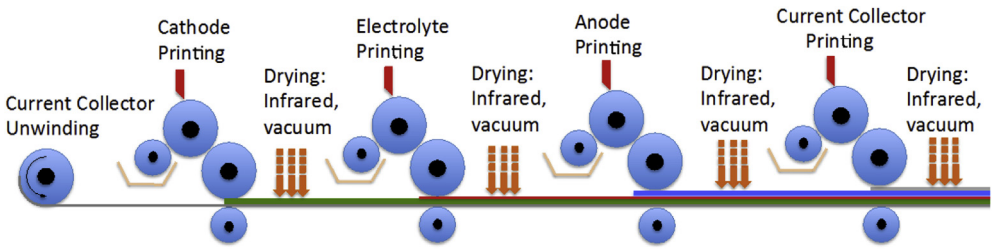

Fig. 1. Proposed multi-station flexographic printing process for large-scale battery production.

Fig. 2. (a) Films printed from commercial flexographic inks on stainless steel foil; (b) poor wetting properties with aqueous based cathode inks on stainless steel foil; (c) non-uniform films printed with NMP-based cathode inks.

filler (Alfa Aesar, CAS1333-86-4, 100% compressed) and 4 wt% extender solutions (Speedball Printing Ink Extender Base).

2.1.3. The NMP-based MnO_2 ink contains 90 wt% activated MnO_2 powder, 6 wt% acetylene black and 4 wt% PVDF-HFP (Kynar Flex 2801). The PVDF-HFP solution was first formed by dissolving one part polymer powder in fifty parts NMP solvents (Sigma Aldrich) before mixing with MnO_2 and AB powders. The mixing was done by placing the ink jars in a high-energy planetary ball mill (Torrey Hills ND 0.4 L) and operating at rotational speeds of 210–280 rpm for 180 min.

2.1.4. The water-based MnO_2 inks with CMC/SBR binder were composed of 90 wt% activated MnO_2 powder, 6 wt% acetylene black (AB), 2 wt% carboxymethyl cellulose, sodium salt (MTI) and 2 wt% styrene-butadiene rubber (MTI). The CMC solution was formed by dissolving one part of powder in ninety parts of DI water. The SBR solution used was a 50% emulsion as received.

2.1.5. The water-based MnO_2 inks with PSBR binder were composed of 90 wt% activated MnO_2 powder, 6 wt% acetylene black (AB), and 4 wt% modified styrene-butadiene rubber (PSBR-100 from Tragray). This PSBR emulsion solution is more viscous than the typical SBR from MTI and provides high binding strength according to the emulsion manufacturer. Water-based ink with dispersing agents was formed by adding one part commercial dispersing agent for aqueous systems (W-28 from Nuosperse) to 7 parts MnO_2 and AB powders. The specific dispersing agent (a non-ionic surfactant) plays a roll of being separator and preferentially adsorbs on the powder surface to provide an effective steric layer, which prevents agglomeration and sedimentation.

2.1.6. The gel electrolyte consists of a 1:1 mixture of PVDF-HFP and 0.5 M solution of zinc trifluoromethanesulfonate ($Zn^+ + Tf^-$ from Sigma Aldrich, 98%purity) salt dissolved in $BMIM^+ + Tf^-$ (from Sigma Aldrich, ≥98.0% purity) ionic liquid. All the raw materials were dried in oven at 100 °C for 24 h before the electrolyte formulation. The 0.5 M ionic liquid electrolyte was first prepared by placing the ink jar on a hot plate for 120 min at 70 °C for a complete dissolution. The mixing of the electrolyte solution with added PVDF-HFP was then done by placing the ink jar in a high-energy planetary ball mill (Torrey Hills ND 0.4 L) and operating at rotational speeds of 210–280 rpm for 180 min.

2.2. Rheological characterizations

Viscosity and yield stress test were performed at 25 °C using a rheometer (HAAKE Rheoscope) with a standard cone and plate geometry (cone diameter = 60 mm, cone angle = 2° and gap = 150 lm). Classic viscosity-shear rate curves were obtained using the steady-state viscosity test. All composite ink samples (typically around 5 ml for each experiment) were initially pre-sheared at 0.1 s^{-1} for 60 s, which was followed by a 60 s equilibration time before conducting the viscosity measurements at shear rate ranges of 0.1 s^{-1} to 1000 s^{-1} increasingly, and each experiment was repeated at least three times for obtaining consistent results. For standard yield stress measurement, five ink samples were initially pre-sheared for 60 s at 1 Pa followed by a 60 s equilibration time before performing a stress sweep from 1 to 300 Pa, over a time period of 300 s. This controlled stress test was repeated three times for each sample to obtain average values and standard deviations.

2.3. Wetting properties measurements

All surface tension measurements were performed using a KSV Sigma 701 tensiometer using the Wilhelmy plate method. Contact angle measurements of the various inks were performed using a photographic method using the custom-built dispenser printer, a technique based on the goniometer method. ImageJ software was used for captured image post-processing and contact angle analysis.

2.4. Ink printability testing

An automated ink proofing system (Perfect Proofer®) was used for developing and testing battery inks at the milli-liter scale.

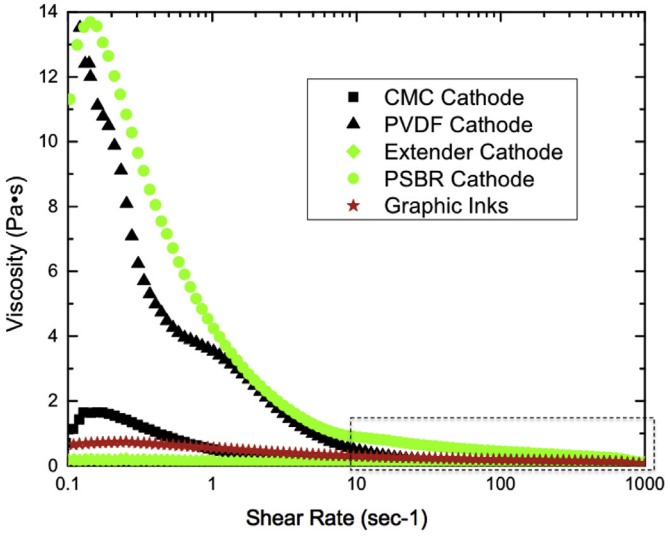

Fig. 3. Viscosity as a function of shear rate for five different types of inks (four developed in this investigation for functional flexographic printing).

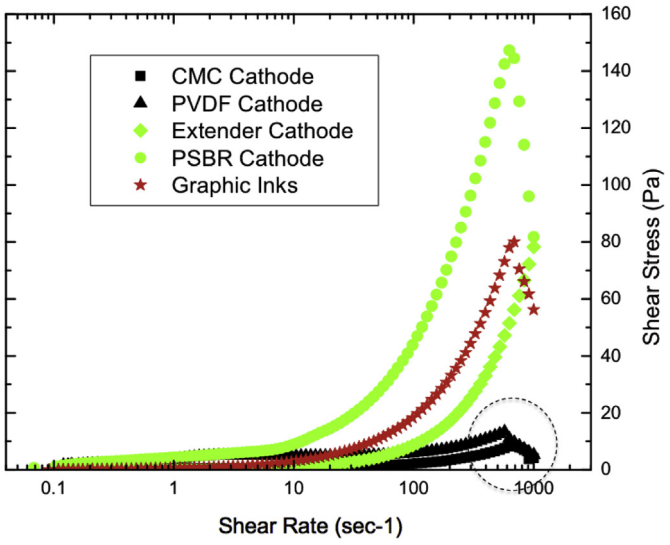

Fig. 4. Shear stress as a function of shear rate for five different types of inks developed for flexographic printing.

2.5. Electrochemical characterizations

Cyclic voltammetry (CV) experiments were performed using a Gamry Reference 600 Potentiostat/Galvanostat/ZRA. Galvanostatic characterizations were conducted with both of the Gamry system and a custom built potentiostat/galvanostat at UC Berkeley.

3. Results and discussion

3.1. Key criteria for developing functional flexographic inks for battery electrode fabrication

3.1.1. Ink rheology

As shown in Fig. 3, all the inks demonstrate shear-thinning behavior to varying degrees. At low shear rate range, the NMP-based PVDF-HFP cathode inks and water-based PSBR cathode inks show higher viscosity than other three inks including commercial flexographic black inks, water-based CMC/SBR cathode inks as well as commercial extender based inks. All ink viscosities decrease with increasing shear rate, and keep below 1 Pa·s from 10 s^{-1} to 1000 s^{-1}, which is the typical operating shear rate range for a high speed flexographic press. This indicates that all the inks should have no difficulties with transfer processes from ink reservoir to foil

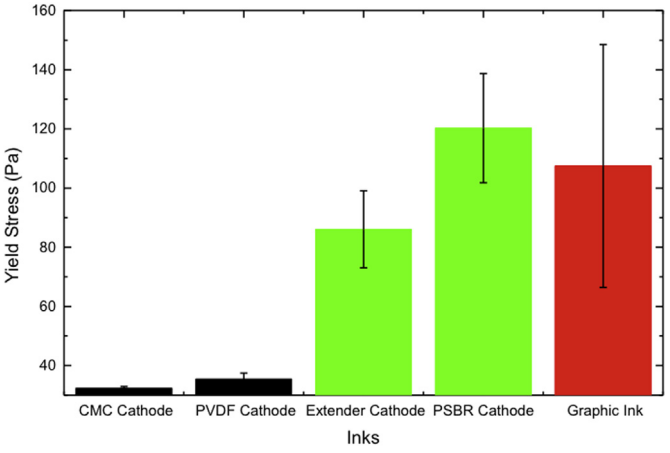

Fig. 5. Yield stress for five different types of inks developed for flexographic printing.

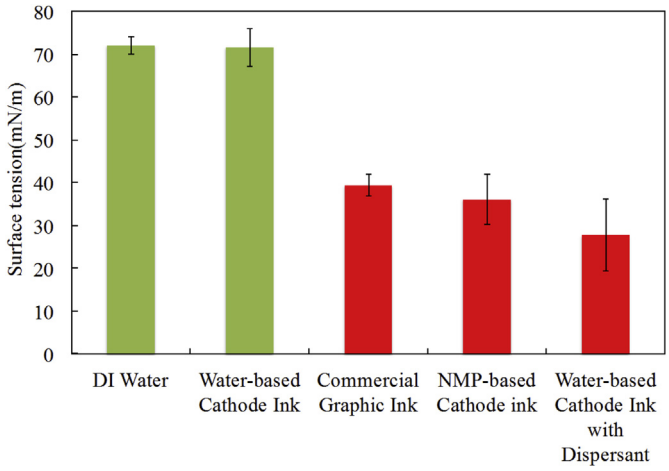

Fig. 6. Surface tensions of water, water-based CMC/SBR cathode ink slurry, a commercial water-based black ink, NMP-based PVDF cathode ink slurry and water-based CMC/SBR cathode ink slurry with dispersants. Dispersing agent has significantly improved the wetting properties of water-based ink on stainless steel substrate.

substrates. However, the plots of shear stress-shear rate from the same sets of experiments in Fig. 4 show substantial difference regarding critical shear stress. The critical shear stress is reached at the peak of each curve. It can be noticed that both of the CMC/SBR cathode slurry and the PVDF-HFP slurry, which gave worse printing quality from printability experiment, show much lower critical shear stress than other three inks.

Standard yield stress measurement results are shown in Fig. 5. Yield stress is found to be a critical parameter, which determines the flexographic ink transition point from a solid-like behavior to a liquid-like behavior in which the composite material's internal network structure starts to break down, and the material begins to flow under shear and compressive stresses after they were transferred to the substrate. [47–49] Due to the low yield stress of CMC/SBR cathode slurry and the PVDF-HFP slurry inks, their internal structure tends to easily get broken. Once a pressure or a shear stress is applied to the inks, active particles could easily be squeezed to the edge of the film causing high non-uniformity as seen in Fig. 2(c). An even worse situation would be that inks flow without control at the edge of the printed area so that the film shape becomes irregular and pattern transfer becomes inaccurate. On the other hand, the PSBR cathode slurry had similar yield stress

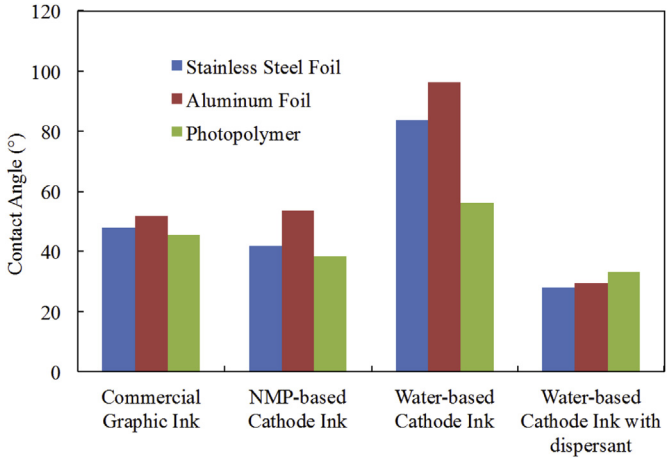

Fig. 7. Contact angles comparison of commercial water-based ink, NMP-based cathode ink, water-based cathode ink and water-based cathode ink with 4% dispersing agent.

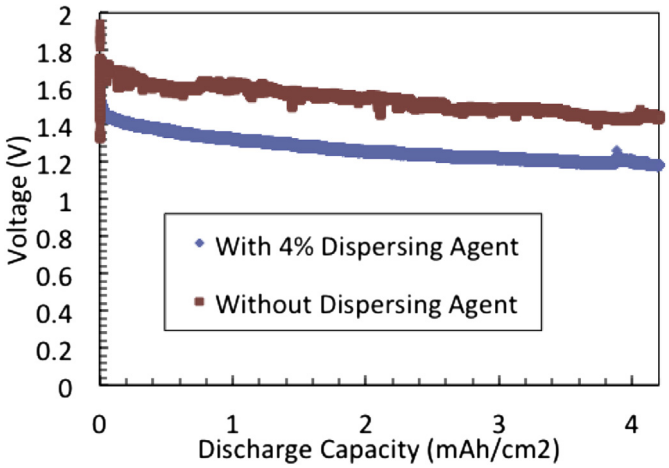

Fig. 8. Comparison of the electrochemical performance of the cathode films printed from inks with and without 4% dispersing agent.

as with commercial flexographic inks as well as extender based electrode inks, so it also achieved very good flexographic printability.

In most of studies of the rheology of fluids, it is quite common to just run steady-state viscosity measurements or even just simple single-point viscosity measurement (at a only one shear rate). For flexographic ink development, a yield stress study is here discovered to be equally, if not more, important due to the nature of the complicated printing process itself. It is concluded that both the viscosity and yield stress of functional flexographic inks need to be well designed to guarantee there are both of a smooth ink flow and an accurate ink deposition as well as pattern transfer. The latter then will also be closely related what will be discussed next: ink wetting properties.

3.1.2. *Wetting properties*

The wetting properties of the functional inks on various substrates are important because they greatly influence the ink adhesion and final feature formation after the flexographic ink gets transferred to the substrates, either before or after the stresses is released from the inks.

The surface tensions of various inks made using the previously described formulations are presented in Fig. 6 below. Both the NMP-based and water-based MnO_2 inks with dispersing agent have shown similar surface tension values to commercial flexographic inks, which are significantly lower than what is measured for pure DI water as well as water-based inks. The value for NMP-based inks is low because the organic solvent, NMP, mainly exposed at the surface of the slurry has much lower surface tension than pure DI water (72 mN m^{-1}). However, by adding dispersing agent consisting of a combination of non-ionic surfactants, even water-based slurry could achieve lower surface tension. The results also indicate the two most effective approaches in order to improving wetting properties of the inks: by controlling the contents of solvent or adding proper amount of surfactant additives.

While surface tension measures the cohesive surface properties of various inks, contact angle gives more direct indication of the interfacial properties between the inks and substrates. Fig. 7 compares the contact angles of the inks on various substrates. NMP-based cathode ink has similar contact angles measured with commercial graphic inks on all three substrates, which implies wetting properties are good. The water-based inks without dispersants, as shown from Fig. 2(b), cannot be printed well due to its high contact angles. However, by adding just 4 wt% of the dispersing agent to the water-based slurry significantly reduced the contact angles to desired values.

3.1.3. *Ink dispersing qualities*

Fig. 8 shows the voltage versus discharge capacity curve from batteries assembled with cathode films flexographically printed with inks with and without 4 wt% dispersing agent. The discharging curve from cathode ink with dispersing agent is much smoother than the one without dispersing agent, which implies that the ink homogeneity and film uniformity are likely to be improved physically through adding surfactant based dispersing agent. From this figure, it can be seen that the non-conductive dispersing agent has

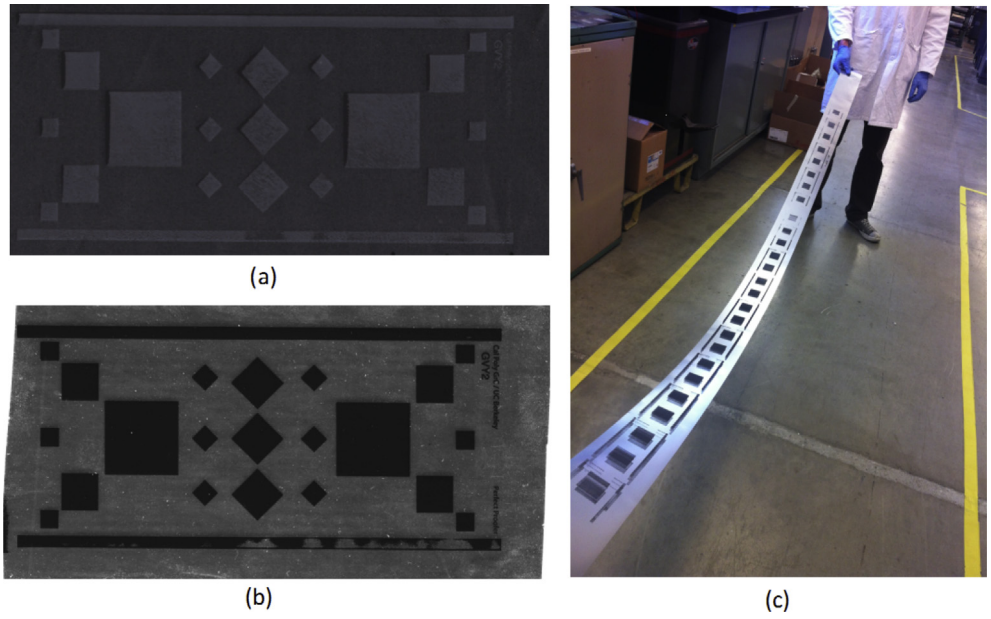

Fig. 9. Significant improvement of printing quality on stainless steel foils by using cathode slurry inks with different polymeric binding solutions: (a) Printed films from MnO_2 cathode ink formulations with CMC/SBR binder; (b) Improved printed films from cathode ink formulations with PSBR binder; (c) Five continuous printed PSBR cathode films on a piece of stainless steel foil.

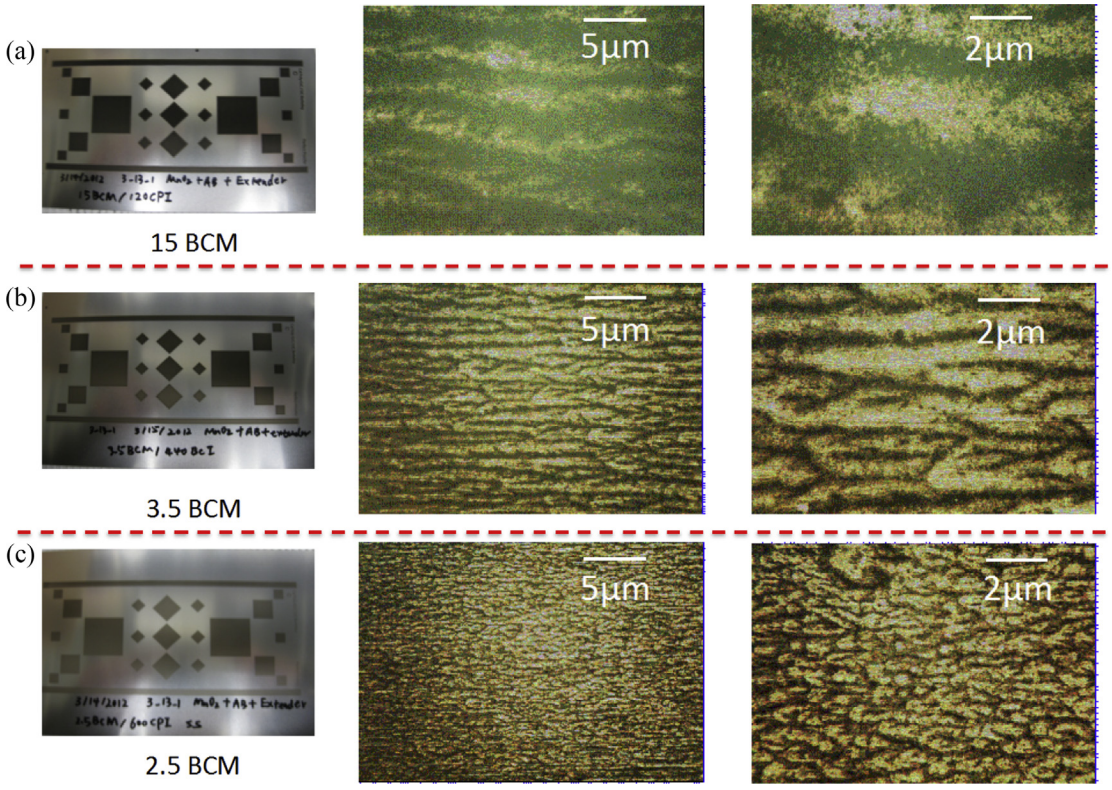

Fig. 10. Flexographically printed PSBR-based cathode films under the optical microscope showing viscous figuring patterns: films respectively printed by using (a) 15 BCM anilox roller, (b) 3.5 BCM anilox roller and (c) 2.5 BCM anilox roller.

increased the internal resistance within the cell, which caused a lower discharge voltage.

3.2. Physical characterizations of flexographically printed films

With the different types of inks presented in the sections above, a series of printability experiments have been conducted. Fig. 9(a) is a representative pattern printed using cathode ink formulations with CMC/SBR binders on stainless steel foils while Fig. 9(b) is a representative pattern from using ink formulations with PSBR binders. Because of the low yield stress from the CMC/SBR cathode inks (similar value with PVDF-HFP cathode inks as shown in Fig. 5), once the ink transferred to the substrate, the major part of the active powders including MnO_2 and acetylene black were easily squeezed to the edge of the pattern that was printed. Instead of forming a uniformly distributed film, this resulted in deposition of "inactive areas" in the battery electrode, which could then cause deteriorated electrochemical performance. With PSBR based inks satisfying the established yield stress and ink structural properties criteria, excellent printing quality with sharp edges and high uniformity were achieved, as shown in Fig. 9(b). Fig. 9(c) shows the flexographically printed PSBR-based MnO_2 films with square patterns after five continuous prints on a roll of stainless steel foil.

Fig. 10 below shows optical microscope images of three representative films printed using the same PSBR-based cathode inks on stainless steel foils, but with anilox rollers with different cell volumes engraved on the ceramic surface. Larger cell volume means more ink will be transferred to the substrate, which then gives

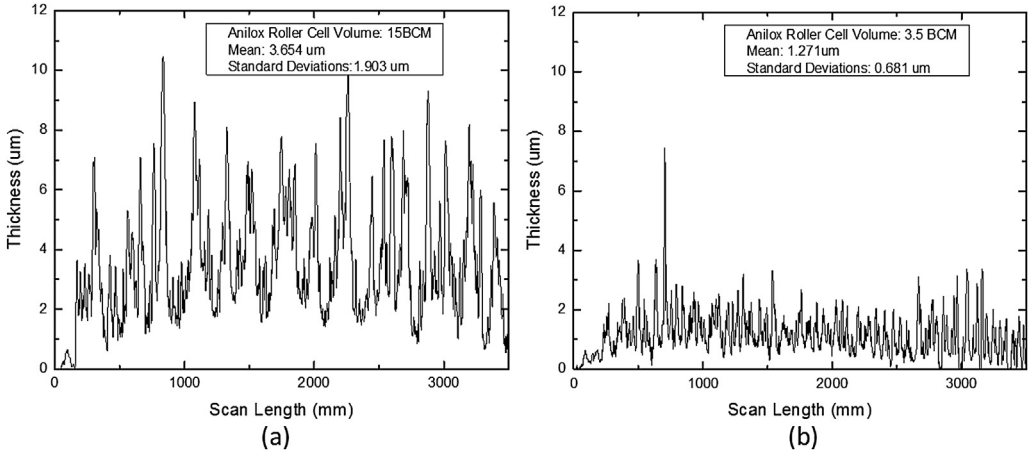

Fig. 11. Surface profile scans of flexographically printed cathode films with: (a) 15 BCM anilox roller, (b) 3.5 BCM anilox roller.

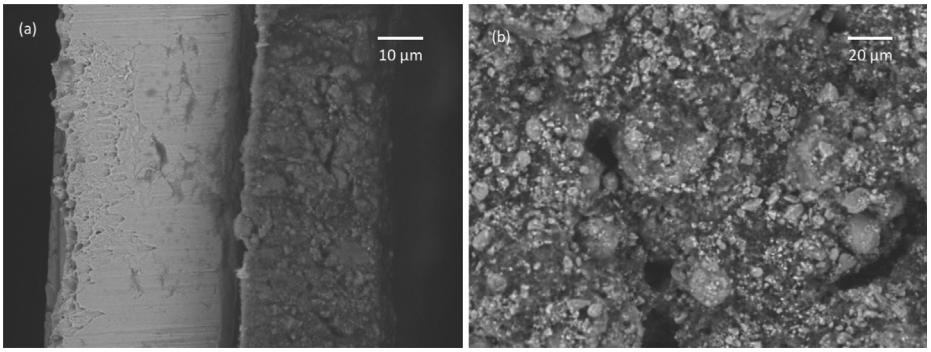

Fig. 12. (a) SEM image shows the cross-section of the printed PSBR MnO_2 cathode films on a current collector foil; (b) SEM image shows the surface profile of a PSBR cathode film.

thicker deposited films. It is observed that all films printed with three available cell volumes show the well-known phenomenon of "viscous fingering" under the microscope. The fingering widths or configurations increase with the larger cell volumes. The fundamental theories of viscous fingering are still not well understood, but it is widely accepted that it is probably due to the instability during the ink transfer process, which causes ink splitting. [50–53] Surface profiles of the printed films are shown in Fig. 11. The anilox roller with 15 Billion Cubic Microns per Square Inch (BCM) cell volume helps achieve a film with an average thickness around 3.654 μm and a standard deviation of 1.903 μm. Anilox roller with only 3.5 BCM cell volume prints a film with an average thickness around 1.271 μm and a standard deviation of 0.681 μm.

For battery electrode printing applications, the thickness typically needs to be at least 20 μm to accomplish desired power and energy output per footprint area. This was realized by running multiple prints based on the same printing substrates. The viscous fingering phenomenon disappeared after running five continuous prints by aligning the plates with the pattern already printed on the substrate as seen in Fig. 12. The cross-section of a film with five continuous printed layers is shown in Fig. 12(a), and an average film thickness around 28 μm was successfully obtained. From the SEM image in Fig. 12(b), it is observed that the water-based cathode film is denser from surface morphology than what was printed from NMP-based cathode. It is probably because of the higher binding strength provided by the PSBR than the PVDF-HFP.

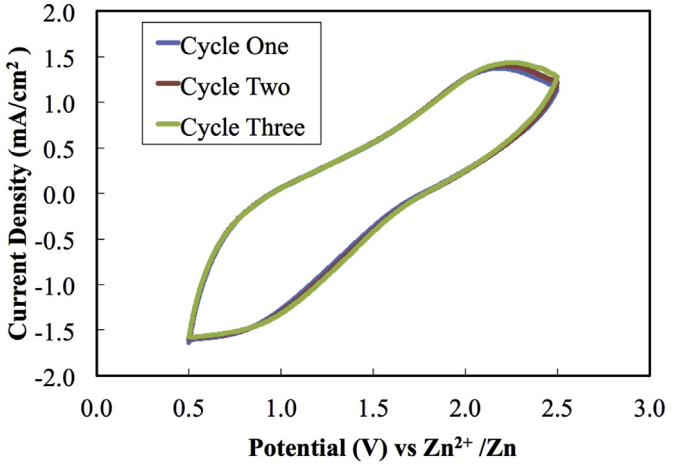

Fig. 13. Voltammogram for a cell consisted of flexographically printed MnO_2 cathode, dispenser printed gel electrolyte, and zinc foil anode at a scan rate of 10 mV s^{-1} for three cycles. Zinc ions insertion into the MnO_2 lattice structure happened when sweeping voltage decreases while zinc ions extraction happened from the cathode structure when sweeping voltage increases. The sweeping direction started towards more positive potentials.

3.3. Electrochemical characterizations

For electrochemical characterizations, gel electrolyte solution was dispenser printed on top of the flexographically printed cathode films. The dispenser printed electrolyte had an active area of 1 cm^2 and an average thickness of 50 μm before being cured in the oven at 70 °C for two hours. Subsequently, a full cell was assembled by placing a piece of zinc foil (from Sigma–Aldrich, 1 mm thickness with 99.999% trace metals basis) on top (pre-cleaned with acetone) and clamping for at least 12 h to equilibrate with the ambient environment before testing. All the assembled cells were tested in ambient environment at room temperature and the results were normalized according to the electrode footprint area the cell occupied.

3.3.1. Reversible zinc intercalation in the flexographically printed MnO_2 cathode

To measure the electrochemical intercalation of zinc ions into the opened layer structure of α-MnO_2 cathode, a two-electrode cyclic voltammetry setup was used for studies of the cells assembled as described above. In these experiments, MnO_2 was the working electrode and zinc foil was used as both the reference and counter electrodes. Fig. 13 shows a representative cyclic voltammetry plot of the insertion/extraction of Zn^{2+} ions into/from the α-MnO_2 cathode through the ionic liquid gel electrolyte at a voltage sweep rate of 10 mV s^{-1} for three continuous cycles. Relatively broad anodic and cathodic current density peaks were detected between 0.5 V and 2.5 V versus the Zn^{2+}/Zn reference electrode,

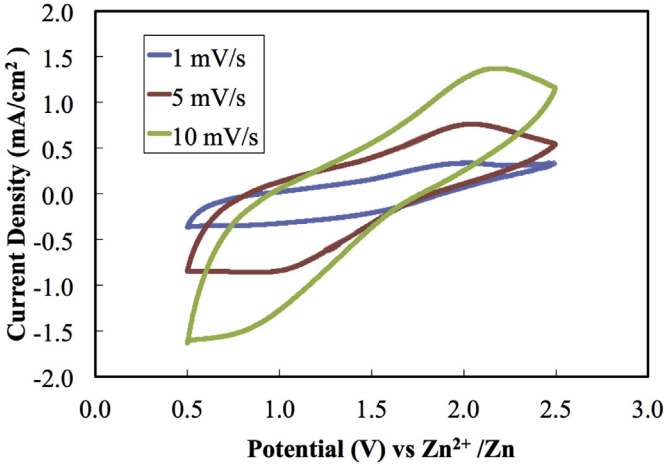

Fig. 14. Voltammogram for an assembled cell consisting of flexographically printed MnO_2 cathode, dispenser printed gel electrolyte, and zinc foil anode at three scan rates respectively: 1 mV s^{-1}, 5 mV s^{-1}, and 10 mV s^{-1}.

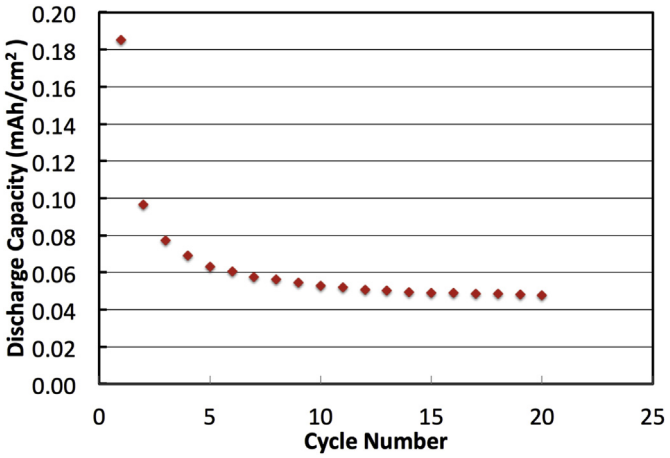

Fig. 15. The galvanostatic cycling of a cell containing flexographically printed MnO_2 cathode, gel electrolyte, and zinc foil anode at a discharge current density of 0.1 mA cm^{-2}.

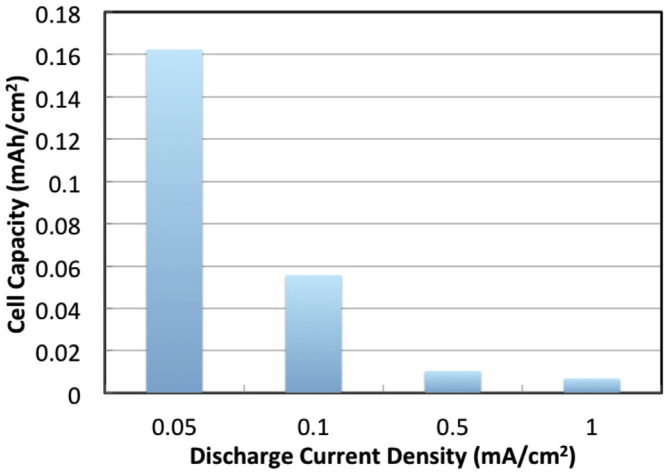

Fig. 17. Discharge capacity extracted from the assembled cell as a function of discharge current density.

which demonstrated the fast transport of zinc ions and high interfacial reaction rate at this voltage sweep rate. The cyclic voltammetry curve indicated that the reversible electrochemical insertion and extraction of Zn^{2+} to and from the MnO_2 films occurred for at least three cycles without cell performance degradation.

3.3.2. Galvanostatic characterization of the flexographically printed MnO_2 cathode

Fig. 14 shows the cyclic voltammetry curves of the flexographically printed cathode at different scan rates. Both reduction and oxidation current density peaks gradually increased with the increasing scan rate. Based on the classical Randles–Sevick Equation, the diffusion coefficient of zinc ions in the PSBR-based MnO_2 cathode is calculated to be about 9.5×10^{-6} cm^2 s^{-1}. For comparison, the diffusion coefficient of zinc ions in BMIM + Tf- ionic liquid electrolytes varies as a function of zinc solute concentrations but is typically of the order of 10^{-8} cm^2 s^{-1} [54].

A typical curve of assembled cell discharge capacity evolution with cycle number at a discharge current density of 0.1 mA cm^{-2} is shown in Fig. 15. The cell was first charged at a constant current density of 0.1 mA cm^{-2} until it reached a cutoff voltage of 1.8 V

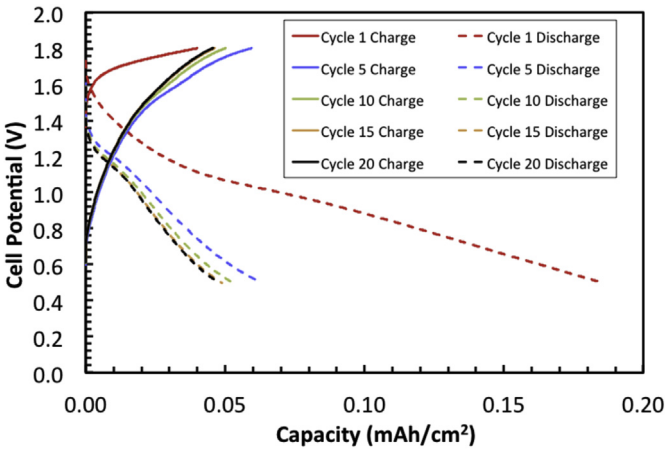

Fig. 16. Cell potential as a function of both depth of charge and discharge for five different selected cycles. The capacity (maximum depth of discharge) drops quickly at the first few cycles but then stabilizes around cycle twenty.

before being discharged between 1.8 and 0.5 V. As can be seen in the figure, the capacity decreased significantly at the first few cycles and then stabilized around cycle twenty. For the first twenty cycles measured, the reversible capacity was approximately 0.05 mAh cm^{-2} while the irreversible capacity was about 0.13 mAh cm^{-2}, about 72% of the first cycle capacity. The irreversible capacity suggested that there was significant loss of active materials with first few cycles of reaction. After twenty cycles, an irreversible capacity still existed throughout each of the following consecutive cycles, but the irreversibility became negligible.

Fig. 16 plots out the detailed cell voltage profile as a function of both the depth of charge and discharge for five different cycles. The Coulombic efficiency of the cell was calculated based on the first twenty cycles, which was about 95% at this discharge rate. This indicated that most of the charged capacity in the cells could be discharged at high efficiency. The active materials utilization of the MnO_2 cathode films was calculated to be around 85%.

Studies on the rate performance of the assembled battery cell were also conducted and the results are shown in Fig. 17. Galvanostatic discharge capacities were measured between 1.8 V and 0.5 V for varying discharge current densities. The cells were charged and discharged using the same protocol as above but at four different current densities respectively: 0.05 mAh cm^{-2}, 0.1 mAh cm^{-2}, 0.5 mAh cm^{-2} and 1.0 mAh cm^{-2}. Fig. 17 shows that the maximum discharge capacity was achieved at the lowest current density 0.05 mAh cm^{-2}, which corresponded to a rate of approximately C/3.2. These results indicate that the printed zinc-based battery based on this specific chemistry works better for energy-related applications in grid storage than power regulating applications. An integrated system with both of the battery and load leveling supercapacitor is widely considered to be able to address the demands for both high energy density and power density systems.

4. Conclusion

A roll-to-roll flexographic printing process for large-scale zinc-based battery manufacturing was proposed. Based on its fundamental operating mechanism, key criteria for developing functional flexographic printing inks were established, including composite ink rheology (steady-state viscosity and yield stress), ink wettability as well as ink dispersing qualities. The ink viscosity significantly influences the ink transfer efficiency while the yield stress critically determines its structural integrity once transferred on

flexible substrate. The ink wettability indicates the ink spreading properties and film uniformity while the ink dispersing quality affects the ink homogeneity from before printing through the printing process. A variety of MnO_2 cathode inks were formulated and analyzed systematically based on these criteria. A novel type of aqueous based cathode ink with PSBR polymeric binder showed excellent flexographic printability. The results of this work are promising for the future development of all other composite slurry components of the zinc-based battery system for flexographic printing as will be shown in future work, including water-based zinc anode, nickel current collector as well as the inert particle-based ionic liquid slurry electrolyte. Future studies will address further optimization of the ink formulations to achieve better printing quality on a variety of nonconductive and conductive substrate. Specifically, the effects of polymeric binder contents as well as the type and amount of surfactant additives on the printability will be interesting.

Extensive electrochemical characterizations with the flexographically printed MnO_2 cathode were conducted. Full cells consisting of dispenser-printed electrolytes and zinc foil anodes were assembled. The cyclic voltammetry method was used to study the reversible zinc intercalation through ionic liquid electrolyte into the aqueous-based cathode. Galvanostatic cycling showed that the cell capacity stabilized after about twenty cycles and the capacity varied significantly with discharge current density. It is important to notice that although the initial zinc-based microbattery experimental results are encouraging, in addition to scaling up the fabrication, the printed rechargeable battery chemistry still needs to be significantly improved in a number of ways. This new chemistry still suffers from a variety of challenging problems, such as capacity fade, low yield and reliability, with contributions possibly coming from both of the materials formulation itself and from the printing process control.

Acknowledgments

The authors acknowledge the support from California Energy Commission for supporting this research under contract 500-01-43. We thank Dr. Jay Keist, Dr. Christine Ho, Bernard Kim, Dr. Reicheng Juang and Dr. Chun-hsing Wu for helpful discussions.

References

[1] E.P. James, M.J. Tudor, S.P. Beeby, N.R. Harris, Sensors Actuators 110 (2004) 171–176.
[2] J. Wilson, V. Bhargava, A. Redfern. Presented at Mobile and Ubiquitous: Networking & Services, Philadelphia, PA, Aug, 2007.
[3] N. Ota, S. Ahrens, A. Redfern, P. Wright, X. Yang. Presented at the Mobile Adhoc and Sensor Systems (MASS). IEEE Inter Conf on, Vancouver, BC, Oct, 2006.
[4] A. Milenković, C. Otto, E. Jovanov, Comput. Commun. 29 (2006) 2521–2533.
[5] S. Roundy, P.K. Wright, J. Rabaey, Comput. Commun. 26 (2003) 1131–1144.
[6] D. Madan, A. Chen, P.K. Wright, J.W. Evans, J. Appl. Phys. 109 (2011) 034904.
[7] A. Chen, P.K. Wright. Modules, Systems and Applications in Thermoelectrics, CRC Pressure, USA, 2012.
[8] L. M. Miller, P. K. Wright, C. C. Ho, J. W. Evans, P. C. Shafer, R. Ramesh. Presented at Energy Conversion Congress and Exposition, IEEE, San Jose, CA, Sept, 2009.
[9] M. Koo, K.-I. Park, S.H. Lee, M. Suh, D.Y. Jeon, J.W. Choi, K. Kang, K.J. Lee, Nano Lett. 12 (2012) 4810.
[10] H. Li, Q. Zhao, W. Wang, H. Dong, D. Xu, G. Zou, H. Duan, D. Yu, Nano Lett. 13 (2013) 1271–1277.
[11] E. Karden, S. Ploumen, B. Fricke, T. Miller, K. Snyder, J. Power Sources 168 (2007) 2–11.
[12] S.M. Lukic, J. Cao, R.C. Bansal, F. Rodriguez, A. Emadi, IEEE Transactions Industrial Electron. 55 (2008) 2258–2267.
[13] J. Cao, A. Emadi, IEEE Transactions Power Electron. 27 (2012) 122–132.
[14] D. O. Energy, Energy Storage-A Key Enabler of the Smart Grid, Sep., 2009.
[15] I. Gyuk, P. Kulkarni, J.H. Sayer, J.D. Boyes, G.P. Corey, G.H. Peek, Power Energy Mag. IEEE 3 (2005) 31–39.
[16] K.C. Divya, J. Østergaard, Electr. Power Syst. Res. 79 (2009) 511–520.
[17] D.H. Doughty, P.C. Butler, A.A. Akhil, Batteries for large-scale stationary electrical energy storage, Electrochem. Soc. Interface (Fall 2010) 49–53.
[18] A.P. Karpinski, B. Makovetski, S.J. Russell, J.R. Serenyi, D.C. Williams, J. Power Sources 80 (1999) 53–60.
[19] J.J. Xu, H. Ye, J. Huang, Electrochem. Commun. 7 (2005) 1309–1317.
[20] C. Xu, H. Du, B. Li, F. Kang, Y. Zeng, Electroche Solid-State Lett. 12 (2009) A435–A441.
[21] C.C. Ho, J.W. Evans, P.K. Wright, J. Micromech. Microeng. 20 (2010) 104009.
[22] P.H. Humble, J.N. Harb, R. LaFollette, J. Electrochem. Soc. 148 (2001) A1357–A1361.
[23] L. Zhang, H. Huang, W.K. Zhang, Y.P. Gan, C.T. Wang, Electrochimica Acta 53 (2008) 5386–5390.
[24] L. R. Erisman, R. A. Marsh, U.S. Patent 4, 091, 1841978, 1978.
[25] K. Kordesh, M. Weissenbacher, J. Power Sources 51 (1994) 61–78.
[26] P. N. Ross Jr, U.S. Patent 4, 842, 9631989, 1989.
[27] S. Müller, F. Holzer, O. Haas, J. Appl. Electrochem. 28 (1998) 895–898.
[28] Z. Wang, A. Chen, R. Winslow, D. Madan, R.C. Juang, M. Nill, J.W. Evans, P.K. Wright, J. Micromechanics Microengineering 22 (2012) 094001.
[29] C.C. Ho, D. Steingart, J. Evans, P. Wright, ECS Trans. 16 (2008) 35–47.
[30] C.C. Ho, D.A. Steingart, J.P. Salminen, Tech. Dig. PowerMEMS (2006).
[31] M. Koplow, A. Chen, D. Steingart, P. K. Wright, J. W. Evans. Presented at the 2008 5th International Summer School and Symposium on Medical Devices and Biosensors, 2008.
[32] A. Chen, D. Madan, B.T. Mahlstedt, P.K. Wright, J.W. Evans, Tech. Dig. PowerMEMS (2010).
[33] A. Chen, M. Koplow, D. Madan, P. K., 2009. Wright, J. W. Evans, Presented at IMECE, 12.
[34] A. Chen, D. Madan, M. Koplow, P.K. Wright, Tech. Dig. PowerMEMS (2009).
[35] D. Madan, A. Chen, P.K. Wright, J.W. Evans, J. Elec Materi 41 (2012) 1481–1486.
[36] D. Madan, Z. Wang, A. Chen, R. Winslow, P.K. Wright, J.W. Evans, Appl. Phys. Lett. 104 (2014) 013902.
[37] D. Madan, Z. Wang, A. Chen, P.K. Wright, J.W. Evans, ACS Appl. Mater. Interfaces 5 (2013) 11872–11876.
[38] D. Madan, Z. Wang, A. Chen, R.C. Juang, P.K. Wright, J.W. Evans, ACS Appl. Mater. Interfaces 4 (2012) 6117–6124.
[39] E.S. Leland, P.K. Wright, R.M. White, J. Micromech. Microeng. 19 (2009) 094018.
[40] B. Johan, US 2688649 A. 1954.
[41] J. B. Story, US 3006980 A. 1961.
[42] B. Bergum, J. Bilhorn, K. Kenyon, W. Macaulay. J. Youngquist, US 3770505 A. 1973.
[43] C.C. Ho, J.W. Evans, P.K. Wright, Tech. Dig. PowerMEMS (2009).
[44] J.H. Lee, U. Paik, V.A. Hackley, Y.M. Choi, J. Electrochem. Soc. 152 (2005) a1763–1769.
[45] J. Li, R.B. Lewis, J.R. Dahn, Solid-State Lett. 10 (2007) A17–A20.
[46] H. Buqa, M. Holzapfel, F. Krumeich, C. Veit, P. Novák, J. Power Sources 161 (2006) 617–622.
[47] J.R. Stokes, J.H. Telford, J. Newt. Fluid Mech. 124 (2004) 137–146.
[48] M.R. Somalu, N.P. Brandon, J. Am. Ceram. Soc. 95 (2011) 1220–1228.
[49] S. Mallik, M. Schmidt, R. Bauer, Presented at Electronics System-Integration Technology Conference, 2008.
[50] S.M. Miller, S.M. Troian, S. Wagner, J. Vac. Sci. Technol. B 20 (2002) 2320.
[51] W.B. Zimmerman, G.M. Homsy, Phys. Fluids A 4 (1992) 2348–2359.
[52] K. Reuter, H. Kempa, N. Brandt, M. Bartzsch, A.C. Huebler, Prog. Org. Coatings 58 (2007) 312–315.
[53] G. Schmidt, H. Kempa, U. Fuegmann, Proc. SPIE 6336, Org. Field-Effect Transistors V. 633610 (2006).
[54] C. C. Ho. Ph.D. Dissertation, May, 2010.